May 9-12
Kyoto-Japan
2017

2nd International Workshop on
Sediment Bypass Tunnels

Mean flow and turbulence variation due to invert abrasion

Christian Auel, Michio Sanjou, Takaaki Okamoto, Sohei Kobayashi and Tetsuya Sumi

Abstract

Due to high bedload sediment transport, many sediment bypass tunnels (SBT) are prone to severe invert abrasion. However, there is little information about the flow characteristics in SBTs after invert abrasion initiated and progresses with time. In the present study, laboratory flume experiments were performed to investigate how the hydraulic conditions change after abrasion patterns developed on the invert. A typical invert abrasion pattern was produced using 3D-printing technique and implemented in the laboratory flume. Flow depths were measured to compare the initial with the abraded state. Furthermore, turbulence measurements using 2D-laser Doppler anemometry technique were performed to obtain the mean and turbulence flow characteristics. This paper describes results of these measurements focusing on the streamwise and vertical flow velocities, turbulence intensities and Reynolds shear stress.

Keywords: 2D-LDA measurements, invert abrasion, Reynolds shear stress, turbulence

1 Introduction

Dams interrupt continuous sediment transport along a river system leading to accumulation in their reservoirs. Sediment bypass tunnels (SBT) are an effective strategy to counteract reservoir sedimentation (e.g., Sumi *et al.* 2004, Auel *et al.* 2016a). Sediments are guided into a tunnel and the reservoir is kept free of sediments downstream of the tunnel intake. The tunnel must be steep enough to transport all sediment without deposition. Due to the resulting high bedload sediment transport, many SBTs face severe invert abrasion (e.g., Auel and Boes 2011). Abrasion is primarily controlled by impacts of saltating bedload particles. Different mechanistic prediction models exist to predict abrasion on both concrete inverts as well as bedrock (e.g., Ishibashi 1983, Sklar and Dietrich 2004, Auel *et al.* 2016b, 2017a, b). These models are based on the physical process of particle impact on the bed.

1.1 Turbulence and invert abrasion experiments at ETH Zurich

In the Laboratory of Hydraulics, Hydrology and Glaciology at ETH Zurich, Switzerland, the spatial and temporal invert abrasion development was analyzed in a scaled model flume representing a straight SBT section (Auel 2014). Furthermore, 2D-LDA

(laser Doppler anemometry) measurements were conducted to analyze the mean and turbulent flow characteristics prior abrasion (Auel *et al.* 2014). The flume bed was partially modeled using weak cement-based mortar mixtures to allow for abrasion. The results showed that bed abrasion progressed with time both in the lateral and vertical direction. Two lateral incision channels developed along the flume side walls at narrow flow conditions occurring at low flume width B to flow depth h aspect ratios B/h < 4-5, whereas randomly distributed potholes were found at wide channels where B/h > 4-5. The observed abrasion patterns matched well with the spanwise bed shear stress distributions found by 2D-LDA measurements on the plain invert prior abrasion (Auel *et al.* 2014). Furthermore, it was found that the abraded mass linearly increased with the transported sediment mass, and abrasion increased with sediment transport rate with highest values for the medium particle diameter category out of three (given a constant sediment supply rate), whereas abrasion decreased with increasing material strength.

1.2 Goals

No detailed information exists about the fundamental physical processes and flow characteristics in supercritical flows after the abrasion process initiated. In the present study, a laboratory experiment was performed in a scaled hydraulic model flume to examine the hydraulic performance of a SBT after invert abrasion. The main objective was to investigate how the mean flow and turbulence structure change after abrasion patterns developed on the invert. The analysis aims to broaden the understanding of the streamwise and vertical flow velocities, turbulence intensities and Reynolds shear stress on complex bed geometries. The present experimental results not only help to develop appropriate design criteria for hydraulic structures to decrease the negative effects of invert abrasion but also provide new insights to the field of geomorphology where similar bedrock erosion processes occur.

2 Methods

2.1 Model setup

We conducted the experiment in a tilting flume at the Environmental Hydrodynamics Laboratory at Kyoto University, Japan. The flume length was 10 m, the width B = 0.2 m and the discharge was Q = 21.6 l/s. One side wall was made of glass to allow for in situ measurements while the bed and the other wall was made of transparent PVC. We simulated one time step of one abrasion experiment (TC2-2) from Auel (2014). The bed slope of the original experiment was S_b = 0.01, while the flow depth at the upstream end of the abrasion section was h = 108 mm, and the Froude number $\mathrm{F} = U/(gh)^{0.5}$= 1.8, with U = streamwise flow velocity, and g = gravitational acceleration (Table 1, column 3). Sediment was supplied with a constant rate of Q_s = 200 g/s using uniform natural sediment of diameter $D \approx 11$ mm. The total run time of the experiment was 930 minutes, while every 60 to 120 minutes the experiment was stopped and the invert

scanned. Here, we modelled one time step of this experiment after 690 minutes run time. As the original flume was 300 mm wide, data had to be downscaled by $\lambda = 1.5$ to meet the facility requirements at Kyoto University (Table 1, column 4). As the flow was not uniform but slightly decelerated in the original experiment, the bed slope had to be adjusted from $S_b = 0.01$ to 0.013 to obtain (approximately) similar Froude numbers and aspect ratios in both experimental setups (Table 1, column 5). The Reynolds number $R = 4R_h/\nu$, with R_h = hydraulic radius and ν = kinematic viscosity, decreased from $R = 4.6\times10^5$ to 2.5×10^5.

Table 1: Experimental data

		ETH Zurich	Scaled ETH	Kyoto University
Experiment		Original TC2-2	λ = 1.5	New
B [mm]	Flume width	300	200	200
L [mm]	Abraded section	1500	1000	1000 (750)
Q [l/s]	Discharge	59.5	21.6	21.6
S_b	Bed slope	0.01	0.01	0.013
x [m]	Start abrasion	10.90	7.27	5.00
h [mm]	Flow depth	108	72	75
B/h	Aspect ratio	2.8	2.8	2.7
U [m/s]	Flow velocity	1.84	1.50	1.44
F	Froude number	1.78	1.78	1.68
R [10^5]	Reynolds number	4.6	2.5	2.5

The abraded invert section was modelled using 3D-printing technique (Figure 1). The original scanned grid of 5 by 5 mm allowed for high accuracy to model the topography. The printed abrasion length was 750 mm out of a maximum possible length of 1000 mm due to economical restrictions. The coordinate system was placed at the center of the flume inlet, with x = streamwise direction, y = spanwise direction and z = vertical direction, while z_0 was the zero-vertical level of the bed prior abrasion (Figure 2).

Both, flow depths and 2D instantaneous velocities were measured at 5 cross sections (x = 4900, 5100, 5300, 5500 and 5700 mm). The flow depths were measured using a point gauge with ±0.25 mm accuracy. The flow depth h_0 was defined from the initial bed z_0 to the (wavy) water surface, and the flow depth h was defined from the abraded bed to the (wavy) water surface (Figure 2). These flow depths were measured (1) prior the installation of the abraded section and were averaged over eight measurements in the spanwise direction at each cross section, and (2) after installation of the abraded section and were averaged over 14 measurements at each cross section.

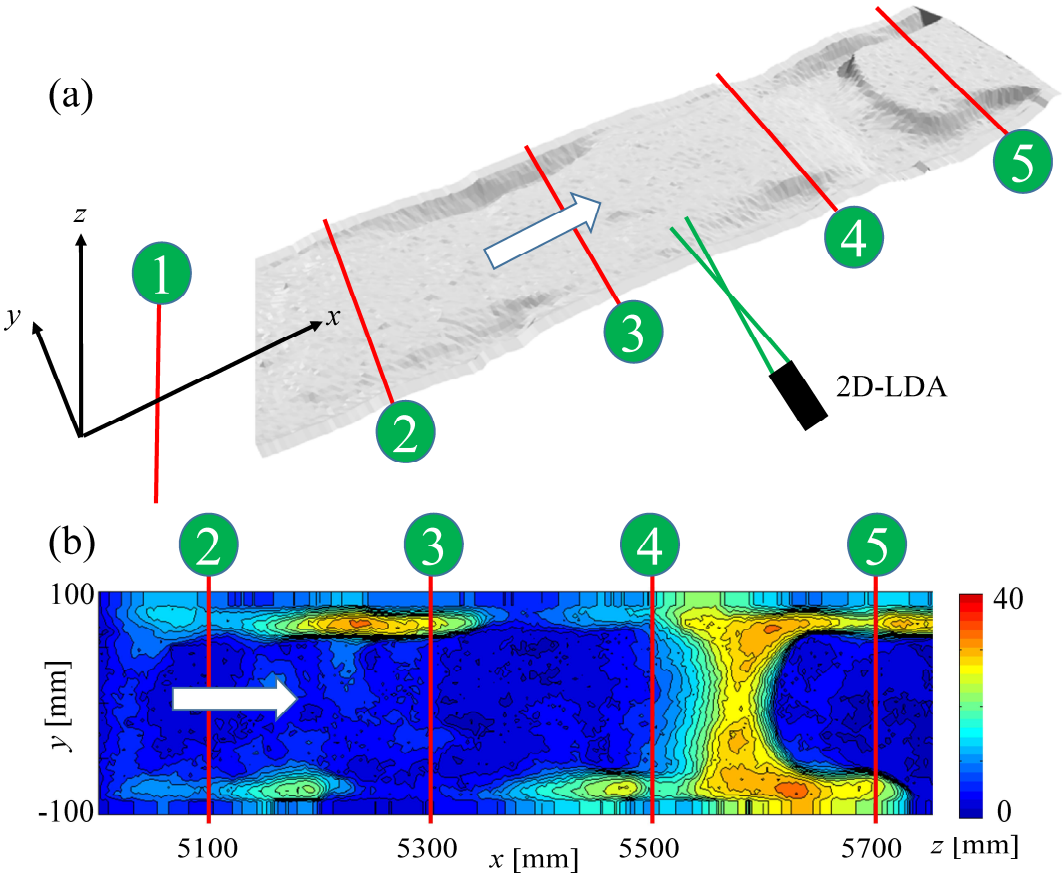

Figure 1: Abraded invert section. a) 3D sketch as printed with 3D printer, b) 2D plan view of original invert from experiment TC2-2 (Auel 2014) after 690 min, downscaled with λ = 1.5. LDA measurements were performed at 5 cross sections.

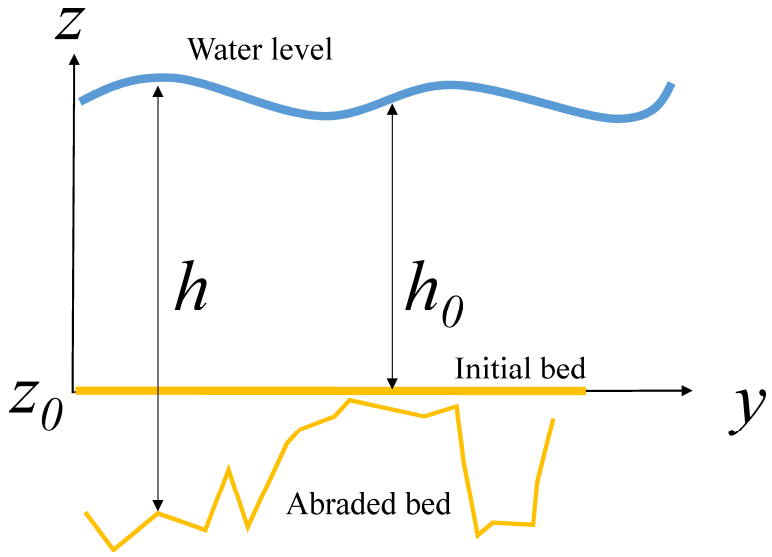

Figure 2: Sketch of flow depth definitions.

2.2 Turbulence measurements

The instantaneous flow velocities in *x*, *y* and *z*-directions are *u*, *v* and *w*, and *u*', *v*' and *w*' are the corresponding velocity fluctuations. The instantaneous velocities are expressed by its time-averaged and fluctuating parts and follow $u(t) = U + u'(t)$, and analogous $v(t) = V + v'(t)$, $w(t) = W + w'(t)$. A two-component fiber-optic LDA system (Dantec Dynamics®) was used to measure the instantaneous velocities in *x* and *z* direction (Figure 3). Movement of the LDA probe in all three dimensions was done with a manual traverse system of 1/100 mm accuracy. At each cross section, we measured 16-24 positions in vertical direction and 12-28 positions in spanwise direction. The sampling time was 120 s per measuring point. Sampling frequency varied between about 1000 Hz near the glass wall while it dropped to about 30 Hz at the PVC wall.

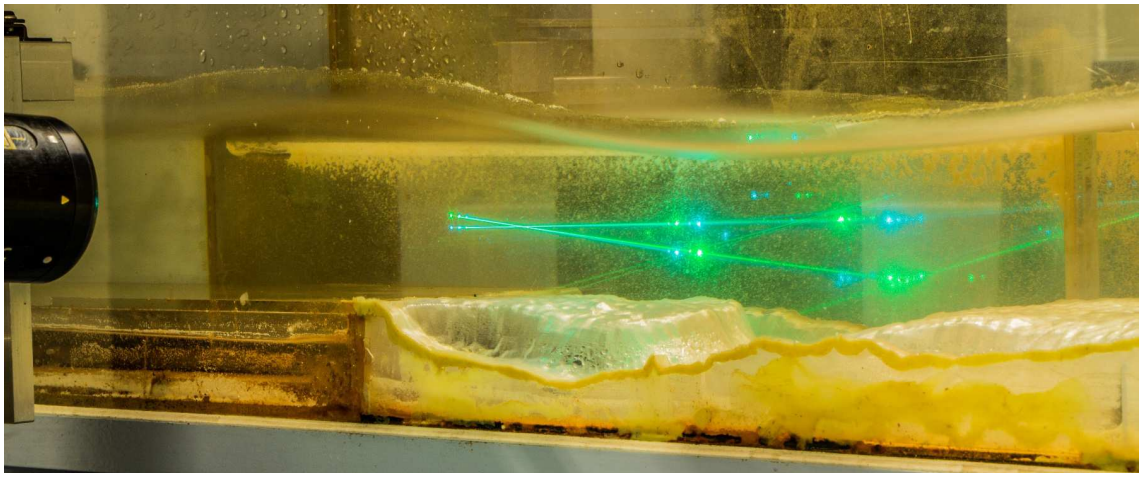

Figure 3: Photograph of the model flume and the 2D-LDA system measuring the horizontal and vertical instantaneous velocities at *x* = 5700 m. Flow direction from right to left (courtesy of C. Auel).

3 Results

3.1 Flow depths

Figure 4 shows both the spanwise-averaged flow depths *h* and h_0 in streamwise direction prior and after abrasion. Evidently, $h_0 = h$ prior abrasion. However, after implementation of the abraded section, the two depths differ considerably. While the flow depths *h* increased due increasing roughness caused by abrasion, the flow depths h_0 decreased. This remarkable result is caused by the bed level changes. The bed abraded deeper than the flow depth *h* increased due to the roughness increase.

Applying these results to a SBT means that no water level rise occurs and hence no increased risk of choking exists once invert abrasion started. However, these results should be verified by more experimental data with different abrasion time steps.

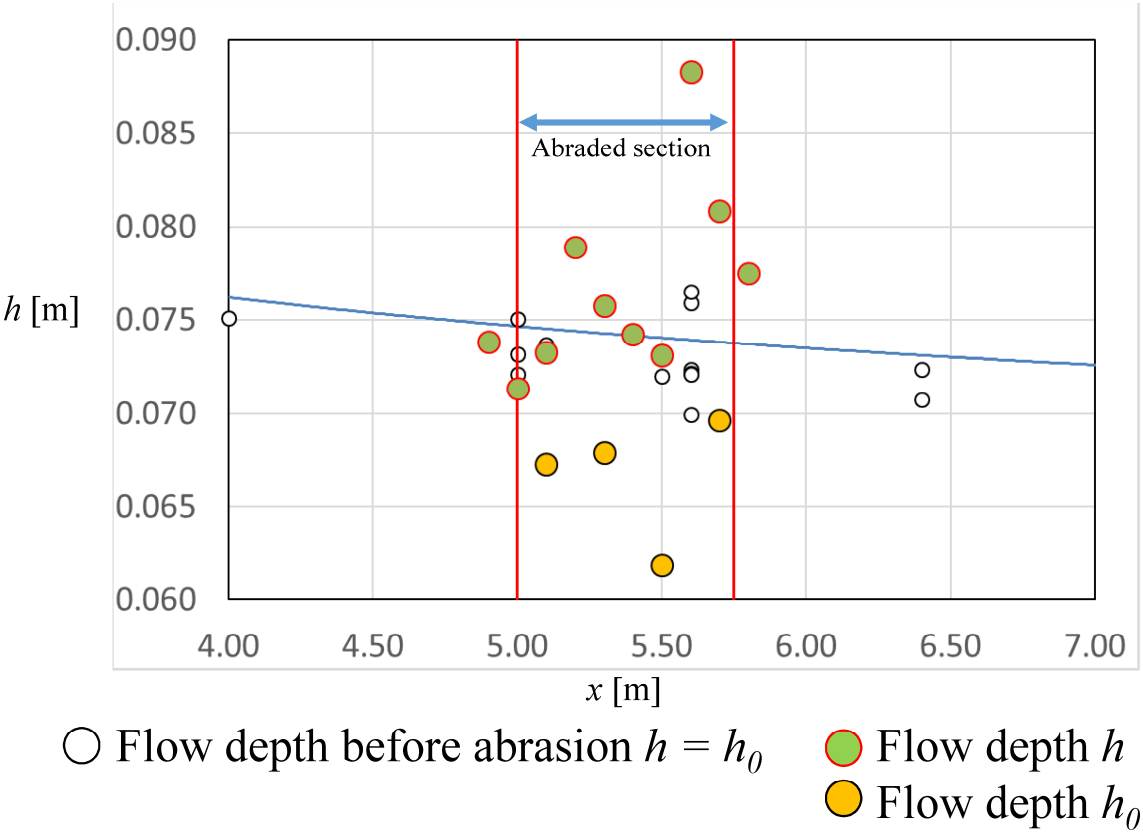

Figure 4: Flow depths prior and after abrasion. The blue line describes the calculated water surface. Figure not to scale.

3.2 Mean flow

Figure 5 shows the contour of the mean streamwise velocity $U(y,z)$ and mean vertical velocity $W(y,z)$ at x = 4900 mm (smooth bed, upstream of the abraded bed section). Both, the ETH (Auel *et al.* 2014) and the Kyoto University data are plotted for comparison; data are scaled with the maximum flow velocity U_{max} and the bulk flow velocity $U_b = Q/(Bh)$, respectively. The maximum streamwise velocity is observed at the centerline and the streamwise velocity decreases in the near sidewall and bottom regions (Figure 5a and c). Strong downward flows occur in the sidewall region, while below the water surface at the flume center, a weak downward flow is observed (Figure 5b and d). Bottom vortices are identified at each side of the flume. These characteristics are present in both flumes and results are hence in good agreement.

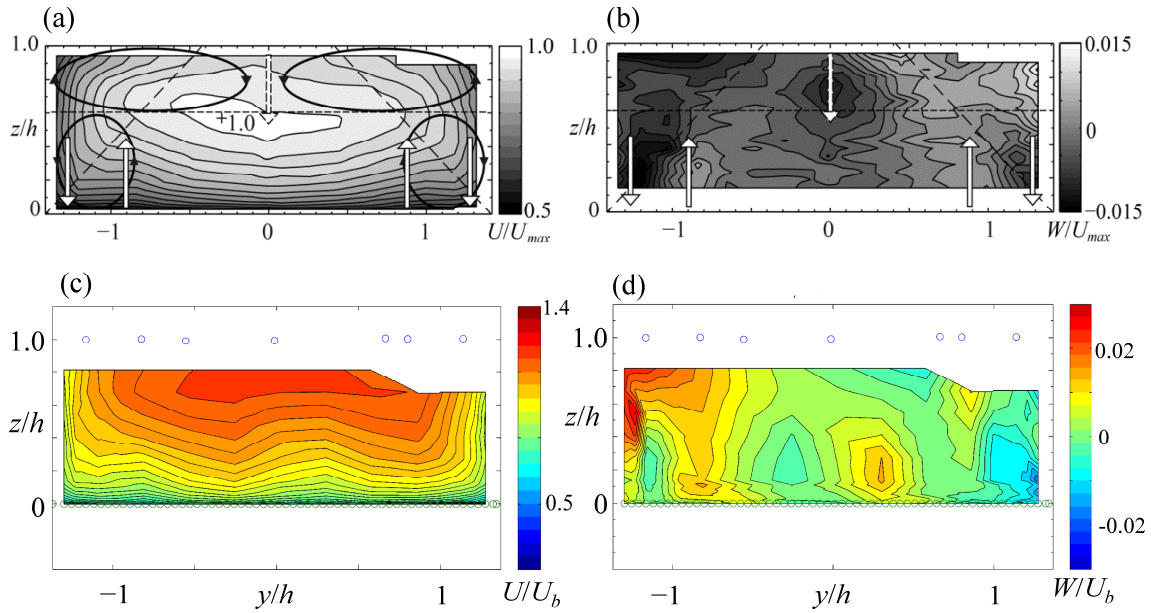

Figure 5: Contour plots of scaled velocity distribution at ETH model flume scaled with U_{max} for a) U = streamwise velocity, and b) W = vertical velocity (Auel *et al.* 2014). Kyoto University flume at x = 4900 m upstream of the abrasion section scaled with U_b for c) U = streamwise velocity, and d) W = vertical velocity. Arrows indicate secondary currents. Blue markers indicate water surface.

Figure 6 and Figure 7 show the contour of the mean streamwise velocity $U(y,z)$ and vertical velocity $W(y,z)$ at x = 5100 mm, 5300 mm, 5500 mm and 5700 mm (abraded bed section). The water surface and bottom profiles are also indicated. The streamwise velocity increases near the flume center while it decreases significantly in the depressed area of the abraded bed (Figure 6). The maximum flow velocities do not occur close to the free surface at $z = h$, but at some distance below z = 0.5-0.8h (velocity dip phenomenon). At x = 5700 mm strong upward flows occur in the sidewall region (Figure 7d). Below the free surface at the flume center, weak downward flow is observed. This indicates that the free surface vortices transport low momentum from the side-wall region to the flume center and bottom region. It is also observed that the strong downward flow occurs in the depressed area of the abraded bed (at y/h = 1.0 and y/h = −1.0). This implies that the abraded bed geometry affects the mean flow structure and the downward flow promotes the bed erosion in the depressed area.

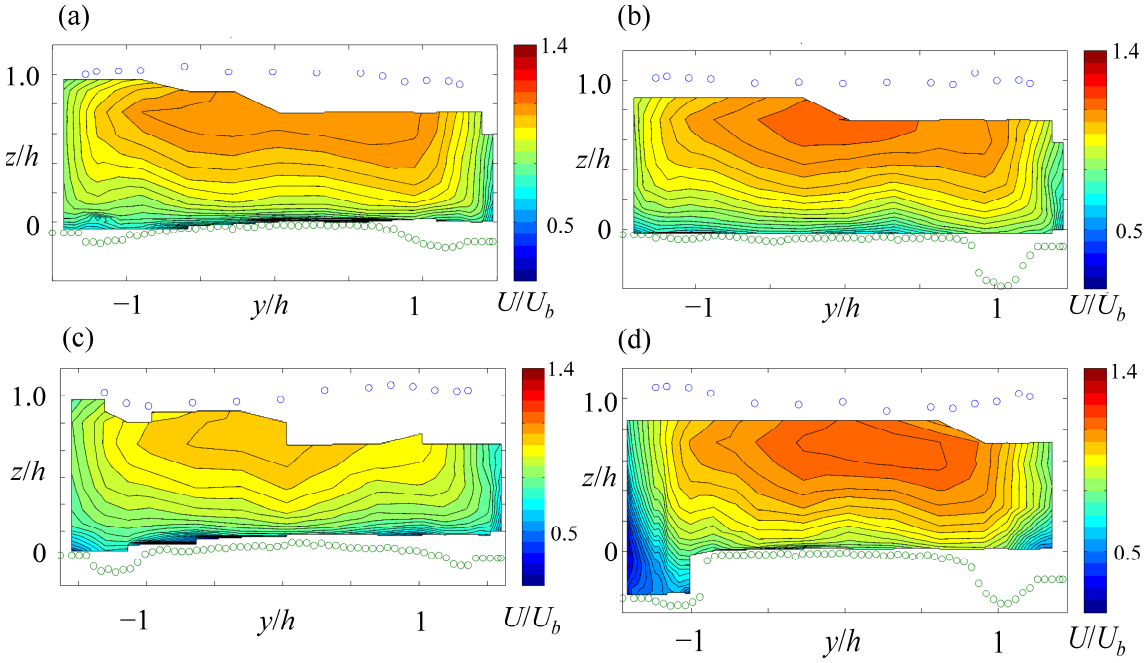

Figure 6: Contour plots of scaled streamwise velocity distribution U/U_b at a) x = 5100 m, b) x = 5300 m, c) x = 5500 m, d) x = 5700 m. Blue markers indicate water surface. Green markers indicate bed.

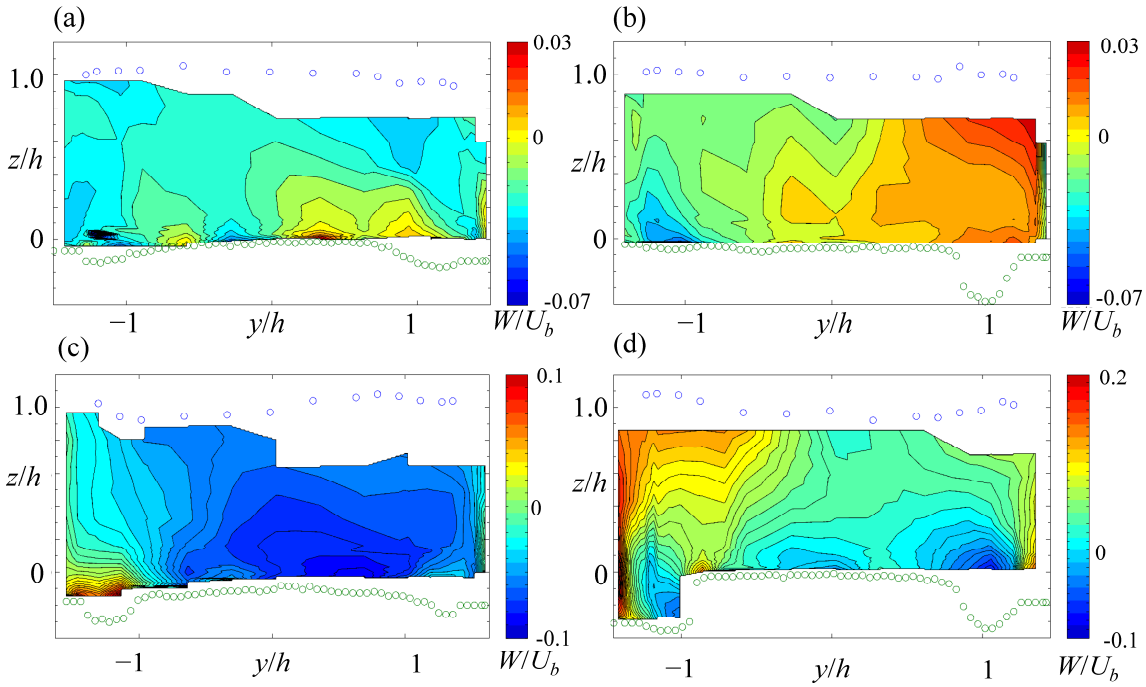

Figure 7: Contour plots of scaled vertical velocity distribution W/U_b at a) x = 5100 m, b) x = 5300 m, c) x = 5500 m, d) x = 5700 m. Blue markers indicate water surface. Green markers indicate bed.

3.3 Turbulent structures

Figure 8 shows the contour of the streamwise turbulence intensity $u_{rms}(y,z)$ and vertical turbulence intensity $w_{rms}(y,z)$ at x = 4900 mm. Both, the ETH (Auel *et al.* 2014) and the

Kyoto University data are plotted for comparison; data are scaled with the friction velocity U_*.

The contours are symmetrical at the corners in the near-bottom region (z/h = 0-0.2). This indicates the existence of bottom vortices along the flume sidewalls. The values of both the streamwise and vertical turbulence intensity increase at z/h = 0.6-1.0 in the near sidewall region. This implies that the free surface vortices have a strong effect on the turbulence intensity. These characteristics are present in both flumes and results are hence in good agreement.

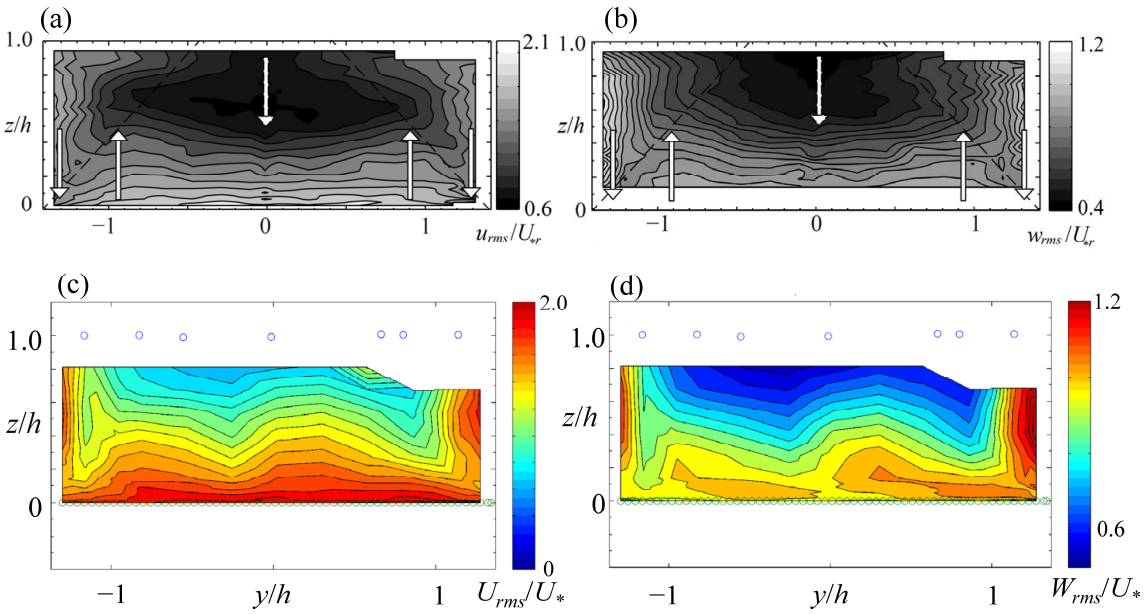

Figure 8: Contour plots of scaled turbulence strength distribution at ETH model flume scaled with U_* for a) U_{rms} = streamwise turbulence intensity strength, and b) W_{rms} = vertical turbulence intensity strength (Auel *et al.* 2014). Kyoto University flume at x = 4900 m upstream of the abrasion section scaled with U_* for c) U_{rms} = streamwise turbulence intensity strength, and d) W_{rms} = vertical turbulence intensity strength. Arrows indicate secondary currents. Blue markers indicate water surface.

Figure 9 and Figure 10 show the contour of the turbulence intensity $u_{rms}(y,z)$ and vertical turbulence intensity $w_{rms}(y,z)$ at x = 5100 mm, 5300 mm, 5500 mm and 5700 mm. The contour values on the abraded bed section are larger than those on the smooth bed, that is at x = 4900 mm. It is also observed that the values of the streamwise and vertical turbulence intensity become larger in the depressed area of the abraded bed. This implies that the abraded bed shape affects the turbulent flow structure leading to high bed shear stress in the depressed area.

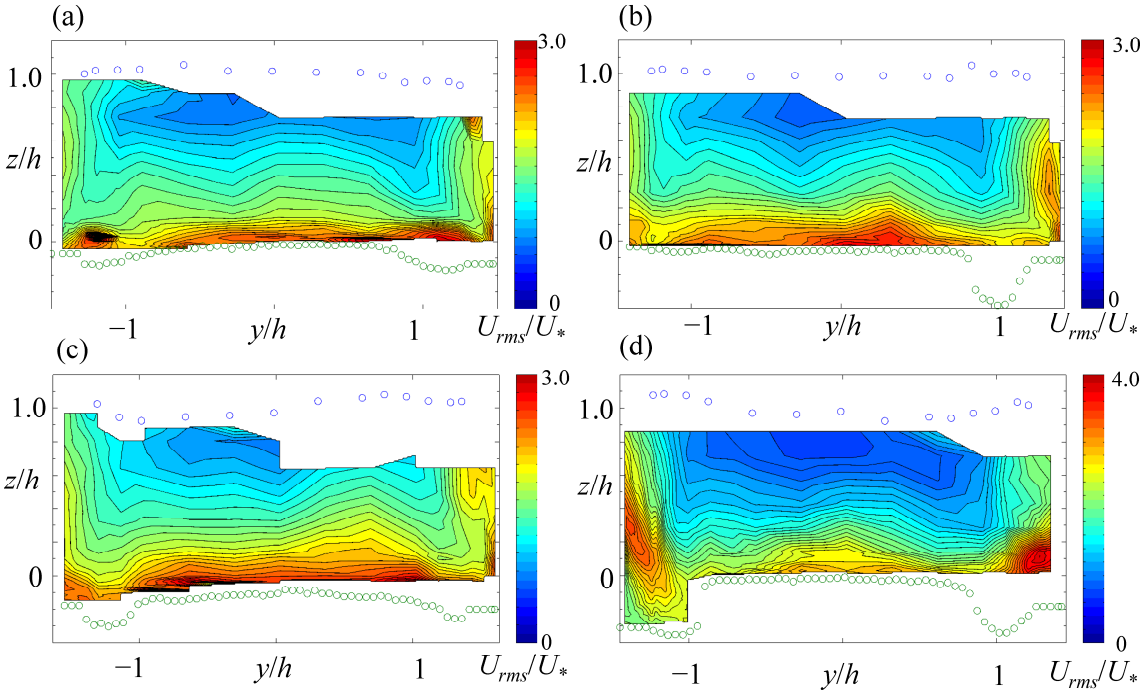

Figure 9: Contour plots of scaled streamwise turbulence intensity strength U_{rms}/U_* at a) x = 5100 m, b) x = 5300 m, c) x = 5500 m, d) x = 5700 m. Blue markers indicate water surface. Green markers indicate bed.

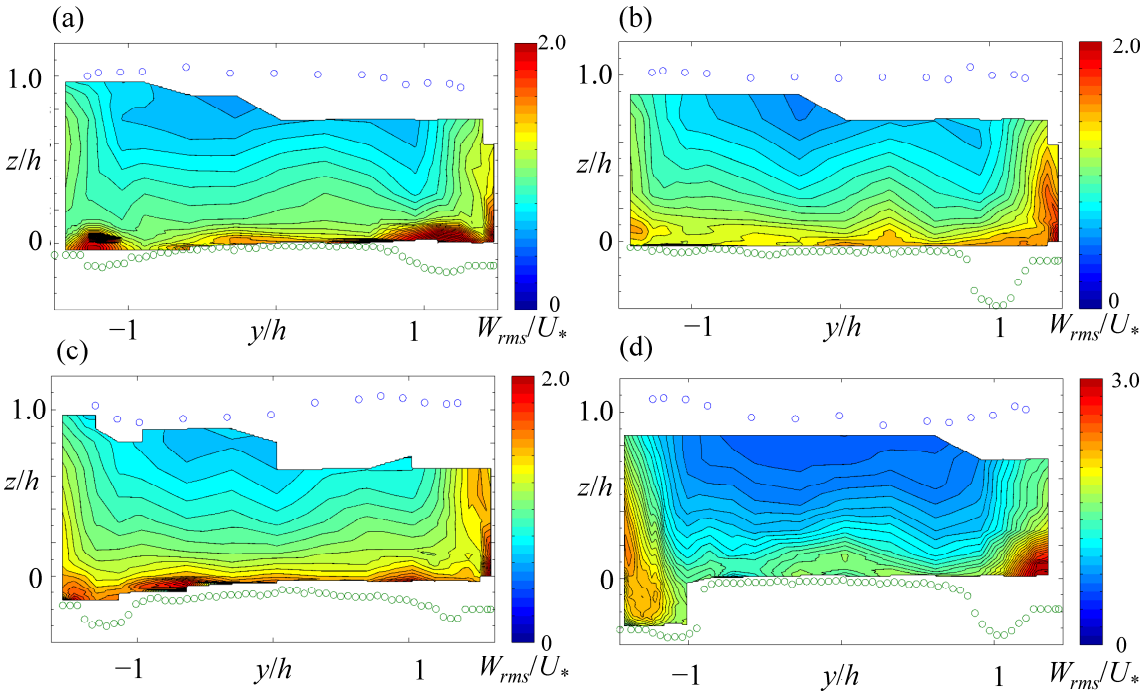

Figure 10: Contour plots of scaled vertical turbulence intensity strength W_{rms}/U_* at a) x = 5100 m, b) x = 5300 m, c) x = 5500 m, d) x = 5700 m. Blue markers indicate water surface. Green markers indicate bed.

Figure 11 shows the contour of the Reynolds stress $-\overline{u'w'}(y,z)$ at x = 4900 mm. Both, the ETH (Auel *et al.* 2014) and the Kyoto University data are plotted for comparison; data are scaled with the squared friction velocity.

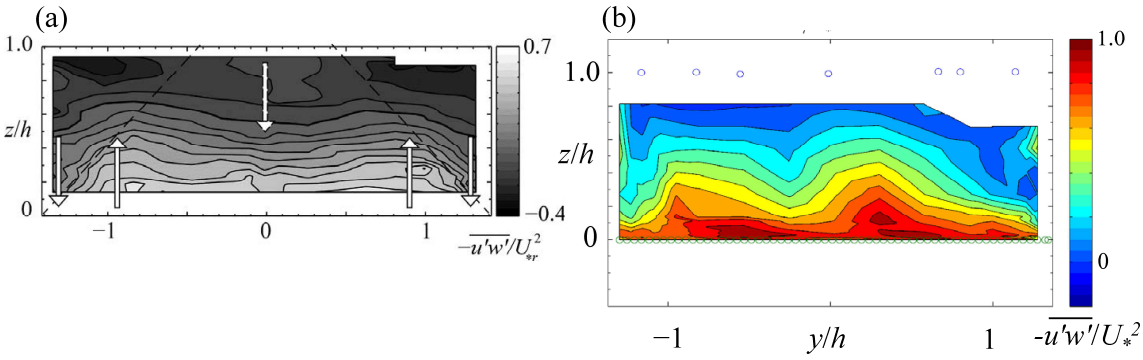

Figure 11: Contour plots of scaled Reynolds shear stress $-\overline{u'w'}/U_*^2$ for a) ETH model flume (Auel *et al.* 2014), b) for Kyoto University flume at x = 4900 m upstream of the abrasion section. Arrows indicate secondary currents. Blue markers indicate water surface.

The Reynolds stress distribution shows a peak value in the near bed region, while they are zero at the flume center (z/h = 0.6-0.8) corresponding well with the location of the maximum streamwise velocity. Large regions of negative Reynolds stress values are observed at z/h = 0.8 in the near sidewall region. This implies the existence of the free surface vortices.

Figure 12 shows the contour of the Reynolds stress $-\overline{u'w'}(y,z)$ at x = 5100 mm, 5300 mm, 5500 mm and 5700 mm. The contour values on the abraded bed sections are larger than those on the smooth bed (x = 4900 mm). Large regions of positive Reynolds stress values are observed at the centerline, while the distribution has negative values in the depressed area of the abraded bed. This confirms that the abraded bed geometry affects the turbulent flow pattern leading to high bed shear stress in the depressed area.

4 Conclusions

In the present study, a laboratory experiment was performed in a scaled hydraulic model flume to examine the hydraulic performance of a SBT after invert abrasion initiated. A typical invert abrasion pattern was implemented in the flume. The abraded section was built with 3D-printing technique. Turbulence measurements using 2D-LDA were performed to obtain the mean and turbulence flow characteristics at supercritical flow conditions. The results are summarized as follows:

1. The velocity dip phenomenon was observed on the abraded bed section. Strong upward flows occur in the wall region. Below the water surface at the flume center, a weak downward flow is observed.

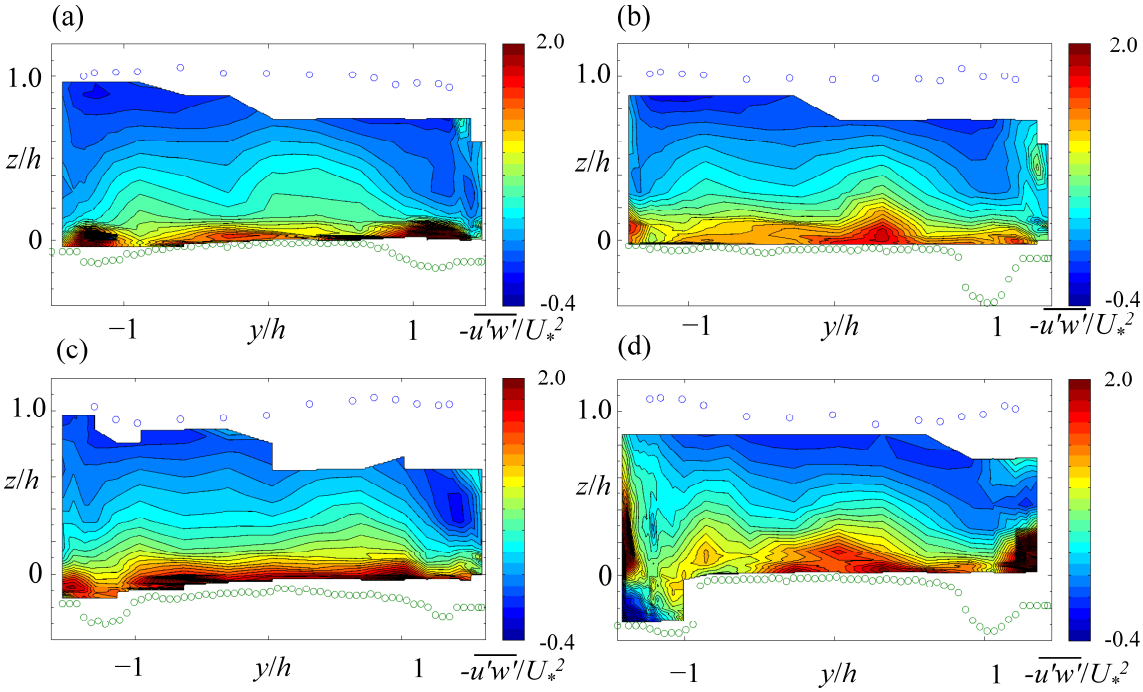

Figure 12: Contour plots of scaled Reynolds shear stress $-\overline{u'w'}/U_*^2$ at a) x = 5100 m, b) x = 5300 m, c) x = 5500 m, d) x = 5700 m. Blue markers indicate water surface. Green markers indicate bed.

2. Strong downward flow occurred in the depressed area of the abraded bed. This implies that the abraded bed geometry affects the mean flow structure and the downward flow is likely responsible for the bed erosion in the depressed area.

3. The contour values on the abraded bed section are larger than those on the smooth bed section. The Reynolds stress distribution reveals negative values in the depressed area of the abraded bed. This confirms that the abraded bed geometry affects the turbulent flow pattern leading to high bed shear stress in the depressed area.

References

Auel, C., Albayrak, I., Sumi, T., Boes, R.M. (2017a). Sediment transport in high-speed flows over a fixed bed: 1. particle dynamics. *Earth Surface Processes and Landforms*. DOI: 10.1002/esp.4128.

Auel, C., Albayrak, I., Sumi, T., Boes, R.M. (2017b). Sediment transport in high-speed flows over a fixed bed: 2. Particle impacts and abrasion prediction. *Earth Surface Processes and Landforms*. DOI: 10.1002/esp.4132.

Auel, C., Kantoush, S.A., Sumi, T. (2016a). Positive effects of reservoir sedimentation management on reservoir life: Examples from Japan. *84th Annual Meeting of ICOLD*, Johannesburg, South Africa 4-11−4-20.

Auel, C., Boes, R.M., Sumi, T. (2016b). Abrasion prediction at Asahi sediment bypass tunnel based on Ishibashi's formula. *Journal of Applied Water Engineering and Research*, DOI: 10.1080/23249676.2016.1265470

Auel, C. (2014). Flow characteristics, particle motion and invert abrasion in sediment bypass tunnels. *PhD thesis* 22008, also published as *VAW Mitteilungen* 229 (R. Boes ed.), ETH Zurich, Switzerland.

Auel, C., Albayrak, I., Boes, R.M. (2014). Turbulence characteristics in supercritical open channel flows: effects of Froude number and aspect ratio. *Journal of Hydraulic Engineering* ASCE 140(4) 04014004, DOI: 10.1061/(ASCE)HY.1943-7900.0000841.

Auel, C., Boes, R. (2011). Sediment bypass tunnel design - review and outlook. Proc. ICOLD Symposium - Dams under changing challenges (Schleiss & Boes, Eds.), *79th Annual Meeting of ICOLD*, Lucerne, Switzerland. Taylor & Francis, London, UK: 403–412.

Ishibashi, T. (1983). Hydraulic study on protection for erosion of sediment flush equipments of dams. *Civil Society Proc.* 334(6): 103–112 (in Japanese).

Sklar, L.S., Dietrich, W.E. (2004). A mechanistic model for river incision into bedrock by saltating bed load. *Water Resources Research* 40(W06301). DOI: 10.1029/2003WR002496.

Sumi, T., Okano, M., Takata, Y. (2004). Reservoir sedimentation management with bypass tunnels in Japan. *Proc. 9th International Symposium on River Sedimentation*, Yichang, China: 1036-1043.

Authors

Christian Auel (corresponding Author)
ILF Consulting Engineers, Rum/Innsbruck, Austria

Michio Sanjou
Takaaki Okamoto
Department of Civil Engineering, Kyoto University, Japan

Sohei Kobayashi
Tetsuya Sumi
Water Resources Research Center, Disaster Prevention Research Institute,
Kyoto University, Japan

Email: christian.auel@alumni.ethz.ch